Advances in Water Resources 192 (2024) 104795

Contents lists available at ScienceDirect

Advances in Water Resources

journal homepage: www.elsevier.com/locate/advwatres

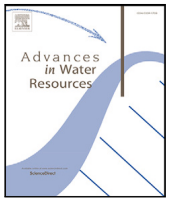

Replication of soil analogues at the original scale by 3D printing: Quantitative assessment of accuracy and repeatability of the pore structural heterogeneity

Janis E. Patiño [a], Filippo Miele [a,b], Alejandro J. Perez [a], Zoe Kanavas [a], Mackenzie L. Dughi [a], Verónica L. Morales [a,*]

[a] Department of Civil and Environmental Engineering, University of California at Davis, United States
[b] Laboratory of Ecohydrology, Ecole Polytechnique Federale Lausanne, Switzerland

ARTICLE INFO

Keywords:
3D printing
Soil
Rock
Pore microstructure
1:1 scale
Permeable
Wettability

ABSTRACT

The present study investigates the quality of four three-dimensional (3D) printing technologies to accurately reproduce the complex pore structure of a real undisturbed soil sample for laboratory experiments of transport in porous media at a 1:1 scale. Four state-of-the-art 3D printing technologies were evaluated (digital light synthesis, PolyJet with gel support material, low-force stereolithography, and PolyJet with water-soluble support material) using a combination of 3D image analysis from microtomography and flow simulations of the pore structure produced with each 3D printing technique. Accuracy, as determined by matching solid and void volumes, permeability, connected porosity, specific surface area, and pore size distribution of the print against the original digital soil structure, was found to be substantially better for digital light synthesis, as compared to the other tested technologies. Repeatability, as determined by the same metrics but compared between identical prints, was found to be comparable across all printing technologies and did not significantly improve for prints at greater magnification (1.5×). Wettability of the samples was improved by plasma treatment of the prints. The thorough analysis herein presented demonstrates that advanced, yet relatively inexpensive 3D printing approaches can be used to generate real-scale high quality analogs of soils/rocks that are much needed for experimental laboratory work. Such a method can open countless opportunities for studying the coupling of pore-structure and hydrodynamics on reactive mass transport in environmental science and engineering, soil science, and other subsurface related fields.

1. Introduction

Geologic media (soils and rocks) are physically heterogeneous; that is, their pore micro-structural properties (e.g., pore size, geometry, alignment, connectivity) can vary greatly in space (Blunt et al., 2013; Bacher et al., 2015; Huang et al., 2011; Meyer and Bijeljic, 2016; Bultreys et al., 2016; Vogel and Roth, 2001). Pore-scale interactions between fluids and geologic media influence numerous subsurface phenomena, including the transport of groundwater contaminants (Zheng et al., 2011), biogeochemical cycling of nutrients (Briggs et al., 2015), storage of CO_2 (Pereira Nunes et al., 2016), extraction of oil from reservoirs (Ishutov et al., 2018b), colloid filtration (Scheidweiler et al., 2020; Bordoloi et al., 2022), and bioclogging (Kurz et al., 2022). The impact of such microscopic physical heterogeneity on macroscopic processes is well documented and recognized for influencing flow distribution (Muljadi et al., 2016; Heyman et al., 2020; Kang et al., 2014), transport behavior (Tompson and Gelhar, 1990; Berkowitz et al., 2000; Morales et al., 2017), mixing dynamics (Werth et al., 2006; Anna et al., 2014; Sole-Mari et al., 2020), fluid partitioning (Benzhong et al., 2019; Ferrari et al., 2015; Bandara et al., 2011) and effective reactions (Meakin and Tartakovsky, 2009; Valocchi et al., 2019; Gramling et al., 2002) that differ substantially from homogeneous media. Nevertheless, a direct and formal relationship between a medium's microscopic structure and its resulting flow and transport dynamics is still elusive. While image-based numerical simulations have been central to elucidating this relationship (e.g., from microtomography scans of the sample), high-quality experimental data is needed to validate and complement the numerical models for flow and transport. Using undisturbed samples for repeatable experimentation is out of the question, as no two natural samples are exactly alike. Methods capable of replicating identical soil/rock pore structural analogues accurately, at high-resolution, in 3D, and at the 1:1 scale, would enable conducting repeatable and well-controlled laboratory experimentation under realistic structural heterogeneity.

* Corresponding author.
E-mail address: vermorales@ucdavis.edu (V.L. Morales).

https://doi.org/10.1016/j.advwatres.2024.104795
Received 10 March 2024; Received in revised form 13 August 2024; Accepted 18 August 2024
Available online 20 August 2024

Significant progress has been made in the last decade to convert digital soils/rocks into 3D printed analogues for geoscience. Resolution and scale are the two most challenging factors for current 3D printing methods aiming to replicate the pore network of natural porous media (Bacher et al., 2015; Otten et al., 2012; Dal Ferro and Morari, 2015; Ishutov et al., 2015, 2021; Kong et al., 2019; Suzuki et al., 2017). The resolution of 3D printing approaches is restricted by the printing technique and the printing material properties. Increasing the scale has been routinely used to capture more details of the structure (e.g., Otten et al., 2012 used 1:3, Ishutov et al., 2018a used 1:15, 1:23, and 1:30, and Song et al., 2021 used 1:10, 1:20, 1:30, 1:60 scale magnification to reproduce 3D printed soil/rock prototypes). An added benefit of upscaling the print is the reduced difficulty in removing residual/support materials from the complex pore network during post-processing, although no reported approach has shown to be fully successful. The latest printing formats like low force stereolithography and digital light synthesis do away with the need for support material altogether, thereby circumventing the issue of pore clogging from inefficient post-processing.

Few studies have successfully reconstructed their undisturbed sample analogues at the original 1:1 scale, albeit with notable limitations. For example, work by Dal Ferro and Morari (2015) printed soil samples at the real 1:1 scale with multijet technology, but reported measured hydraulic conductivity discrepancies from the original soil model of 88%–1400%. Bacher et al. (2015) created reprints of undisturbed soils at their original scale with selective laser sintering, stereolithography, and polyjet approaches, but only reproduced the percolating macropore. Most recently, Ishutov et al. (2021) proposed a two-photon lithography approach that can resolve porous medium features in the order of ~100 nm, with the explicit stipulation about size limitations of the nano-printed model being <1 mm in each direction for a printing job that requires several days of labor.

As of yet, a substantial trade-off exists between achieving accurate pore structures and realistic surface properties in 3D printed soil/rock analogues due to the availability of materials used to print. On the one hand, powder-based printed rock proxies with wettability or reactive surface properties that mimic natural samples suffer evident printing defects with regards to the complex pore structure (Ferrari et al., 2022; Anjikar et al., 2020; Song et al., 2021). On the other, resin-based prints show superior performance at reproducing the complex pore structure but differ in wettability (are typically less hydrophilic) from natural rocks (Song et al., 2021; Dal Ferro and Morari, 2015; Bacher et al., 2015; Ishutov et al., 2021). Recently, different chemical treatments (silanization) have been used to manipulate the wettability of printed porous media with remarkable success in pseudo-2D samples (Catterton et al., 2021; Bacha et al., 2021) or 3D samples with highly homogeneous, and well connected structures made of large pores (>250 μm) (Hodder and Nychka, 2019; Vogelsang et al., 2022). Alternative protocols must be developed for complex samples with structural heterogeneity and micron-sized pores to work around mass diffusion limitations that prevent homogeneous functionalization of the printed surface.

This study explores the quality performance of four low-cost 3D printing technologies to reproduce the heterogeneous pore structure of an undisturbed soil sample at its original 1:1 scale for fluid flow experimentation. We propose specific measurements to benchmark the characteristics that define *accuracy* and *repeatability* in 3D prints from a combination of structural and hydrologic properties obtained from analysis of tomographic images of the printed products and image-based simulations, respectively. The paper is organized as follows. First, we describe the soil model used as the basis for 3D printing, the printing technologies chosen, as well as structural and hydrologic properties considered for evaluating the goodness of the prints. Second, we summarize our evaluation of accuracy and repeatability for the four technologies. Third, wettability of the prints is assessed prior to and post plasma treatment. Finally, we discuss performance trade-offs between the 3D printing technologies evaluated, make recommendations for achieving the most accurate and repeatable porous media analogues, and summarize the limitations of replicating key properties in soils/rocks by 3D printing that are of paramount importance for fluid flow and mass transport.

2. Materials & methods

2.1. Soil model from 3D μCT image

An undisturbed sample of sandy loam Cambisol from an agricultural experimental plot at the James Hutton Institute, Invergowrie, Scotland (established in 2003) was selected as the basis for 3D printing, from here on forth referred to as soil Computer Aided Design (CAD). Characterization of the internal pore geometry was achieved by scanning the sample with 3D micro-computed tomography (μCT) in a Metrix X-Tek X-ray (Nikon, UK) at a resolution of 35 μm. For more details, the reader is referred to Pérez-Reche et al. (2012). A subsample of the segmented scan (size: 14 mm × 14 mm × 18 mm) was selected and pre-processed to remove isolated pores that encumber 3D printing and analysis of the prints. A mesh file of the cleaned soil image was generated with Fiji (Fiji is ImageJ) (Schindelin et al., 2012), an open source image processing software, and exported as a stereolithography (.stl) file for 3D printing.

2.2. 3D printing of soil samples

The four additive technologies considered for 3D printing soil analogues include (1) digital light synthesis (DLS), (2) PolyJet with gel support material (PJ Gel), (3) low-force stereolithography (LFS), and (4) Polyjet with water-soluble support material (PJ WS). The authors note that selective laser sintering (SLS) with nylon powder and stereolithography (SLA) with dual resin were also tested, but were excluded from this study because it was impossible to remove unsintered powder and support resin, respectively, from the pore space (data not included). As a result, the choice of techniques here presented is motivated by the requirement to fabricate a soil analogue with an *open pore space* with as much resolution as possible and at its original scale. Neither DLS nor LFS require a support resin to be used in the void space during printing due to the light sheet used to cure the printing material and their gravity-inverted extraction process (see Fig. A.6 for a schematic). Conversely, both PolyJet approaches (PJ Gel and PJ WS) require the use of a support material for the void space, which require heat and water treatments during post-processing, respectively, to be removed from the pore space. Despite these advantages over solid resin support (e.g., from SLA), gel and water soluble support materials can still be difficult to remove completely. To evaluate improvements in support resin removal, replicates of these techniques were also printed at 1.5× magnification. Samples generated by LFS were printed at two orientations of 45° rotation over an edge or a corner. It is worth noting that LFS prints at the default face (0° rotation) did not generate connected pore networks from the sample's top to bottom, suggesting that rotation during printing is required with this technique.

A summary of the technologies and materials used in each case is provided in Table 1. Details about the principles behind each printing process and a photograph of the produced prints are also included in the appendix (see Appendix A and Fig. A.7). All four techniques here evaluated employ plastic resin as the primary printing material because it provides the best resolution for the final product (Ishutov et al., 2021) and surface finishes (Kafle et al., 2021). Resin is also the most commonly used material for 3D printing (Arrieta-Escobar et al., 2020). Polyjet was chosen because it is one of the most commonly used printing technologies for producing models in the soil science domain Arrieta-Escobar et al. (2020). LFS from FormLabs was chosen because it is a high-quality, high-precision desktop printer found in many classrooms and labs. DLS was chosen for its proclaimed accuracy.

Table 1
3D printing technology specifications for Digital Light Synthesis (DLS), PolyJet gel (PJ Gel), Low-Force Stereolithography (LFS), PolyJet water soluble (PJ WS).

Printing technology	Maker	Material		Resolution[a]	Accuracy[b]	Provider
		Print	Support	XY, Z [μm]	[μm]	
DLS	Carbon M2	UMA90	None	75, 25	70	Diversified Plastics[c]
PJ Gel	PolyJet 3D	VeroWhite HQ	SUP705	16, 16	100–200	Fathom
LFS	Form 3L	Clear Resin	None	25, 25	100–300	UC Davis TEAM
PJ WS	PolyJet 3D	VeroWhitePlus	SUP706	16, 16	100–200	Stratasys

[a] Z resolution is generically reported as the smallest layer thickness.
[b] Manufacturer estimated on closeness agreement between a CAD source file of regular shapes (e.g., pipe, tubes, stair lattice) and the printed product.
[c] DLS replicates were printed by two different providers–UC Davis TEAM and Diversified Plastics.

Identical printing conditions were used for printing at least two replicates for each technology to evaluate repeatability at 1× magnification of the original soil CAD. The cost for fabricating the samples in this study ranged from 50–160 US dollars per unit. All 3D printing services used (three of which are commercial) proposed cost advantages for jobs with 10 or more identical prints, making the technology broadly accessible and affordable for researchers.

2.3. Image analysis of 3D printed soils

2.3.1. 3D microtomography imaging:

3D X-ray microtomography images of each printed sample were collected at a voxel resolution of 25 μm with a MicroXCT-200 (ZEISS Xradia). Scanning settings included 8 W of X-ray power source, 40 kV of energy and 1600 projections covering the full sample at 360°. An LE1 source filter of 0.03 mm thickness was used to reduce beam hardening artifacts (ZEISS X-ray Microscopy, Oberkochen, Germany). Reconstructed images were processed in Amira (Thermo Fisher Scientific), a commercial software for CT image analysis, according to the following protocol for increasing signal-to-noise ratio with a non-local mean filter, registration, rescaling, and segmentation. Given that the microtomography images of the original undisturbed soil and each printed soil analogue varied slightly in scale, orientation, and resolution, two important image pre-processing steps were performed. First, all tomograms were aligned to a common spatial reference by way of image *registration*. Second, all images were matched in resolution by way of image *rescaling* so as to obtain the same voxel size. Finally, watershed thresholding was used to segment the image into solid and pore voxels. The authors note that any support material or residual resin that was not removed by post-processing of the prints was here classified as part of the solid phase. By matching the orientation and resolution of all images it is possible to equitably compare structural properties between and across samples.

Identification of the percolation path (PP) and its morphological characteristics for all sample images was carried out with the Particle Analyzer plugin of the software Fiji (Domander et al., 2021b). Briefly, the Particle Analyzer plugin identifies individual *particles* in the binary image stack, and computes their volume and bounding rectangle dimensions. Here, *particles* correspond to isolated pores that do not necessarily connect all the way through the sample in the z-direction (from the top to the bottom). Only those pores with the largest volume and a bounding rectangle that spans the full length of the sample are taken as the percolation path (PP) (see Fig. B.8). Analyses related to the permeability, specific surface area, connected porosity, and pores size distribution are carried out only on the PP, as it is expected that pores that are not connected to it will not significantly contribute towards flow and mass transport (Sirivithayapakorn and Keller, 2003).

2.3.2. Quantitative image analysis:

The following describes the five quantitative metrics used to evaluate the accuracy and repeatability of the 3D printing technologies because they play important roles in the description and understanding of flow and transport through porous media. The choice of metrics is motivated by the need to balance hard-line criteria for microscopic defects with effective macroscopic performance metrics of hydrologic relevance.

Match/mismatch volume: Voxel-by-voxel comparison between registered and rescaled images is used to provide a volumetric approximation of the *accuracy* across 3D printing technologies (comparing images of 3D printed samples against the reference soil image) and of the *repeatability* within each technology (comparing replicate images of 3D printed samples against one another). Mismatched voxels in analyses for accuracy can be classified in one of two ways. First, solid voxels in the reference soil image that appear as pore in the printed soil are considered *missing*. Second, pore voxels in the reference soil image that appear as solid in the printed soil are considered *excess*. Mismatched voxels in analyses for repeatability have only a single classification, *mismatch*, since there is no reference. Matched voxels for both accuracy and repeatability analysis have the same classification (solid or pore) in the two images being compared and are considered *match*.

Permeability: Permeability defines the ability of the medium to transport fluid. The permeability of each printed soil is calculated from steady-state pore-scale flow simulations (by solving the Navier–Stokes equations) within the porous medium's detailed geometry. The pore geometry provides the local boundary conditions that control the flow field. Direct numerical simulations are then performed with the FlowDict module in Geodict, a commercial solver for porous materials (Math2Market, Germany). Briefly, a mean approach fluid velocity of 25 mm/h (corresponding to a creeping flow with Reynolds number of roughly 10^{-2}, typical infiltration rate for sandy loam soils) is specified in FlowDict (Brouwer et al., 1988). The software adjusts the pressure drop until the calculated water velocity matches the one specified by the user. Then, during post-processing, the software applies Darcy's principle to compute the sample permeability from the simulated mean flow velocity, the water viscosity, simulated pressure drop, and the media thickness (Hilden et al., 2019).

Specific surface area: The specific surface area (SSA) of the pore space is an informative metric for reactive transport problems where reactions occur at the fluid-solid interface (e.g., colloid filtration, mineral precipitation). The SSA is estimated as the surface area to volume ratio of the percolating path, as determined from morphological analysis of this region of interest using the Particle Analyser plugin in Fiji (surface resampling = 1) (Domander et al., 2021a). Consistent and limited resampling on the registered and rescaled images allows a fair comparison of the meshed surface area across samples.

Connected Porosity: Connected porosity is a fundamental metric that describes the fraction of voids in the medium that control the transport of fluids. The connected porosity is computed according to the pore space volume associated with the percolating path, relative to the total sample volume.

Pore size distribution: The pore size distribution is a basic characteristic of porous media that describes its structural heterogeneity and signals the system's propensity for anomalous transport (Xiong et al., 2016). Porosimetry is used to estimate the pore size distribution in each sample with the PoroDict module in Geodict. With this method, the intrusion of a non-wetting fluid is simulated into the pore space and

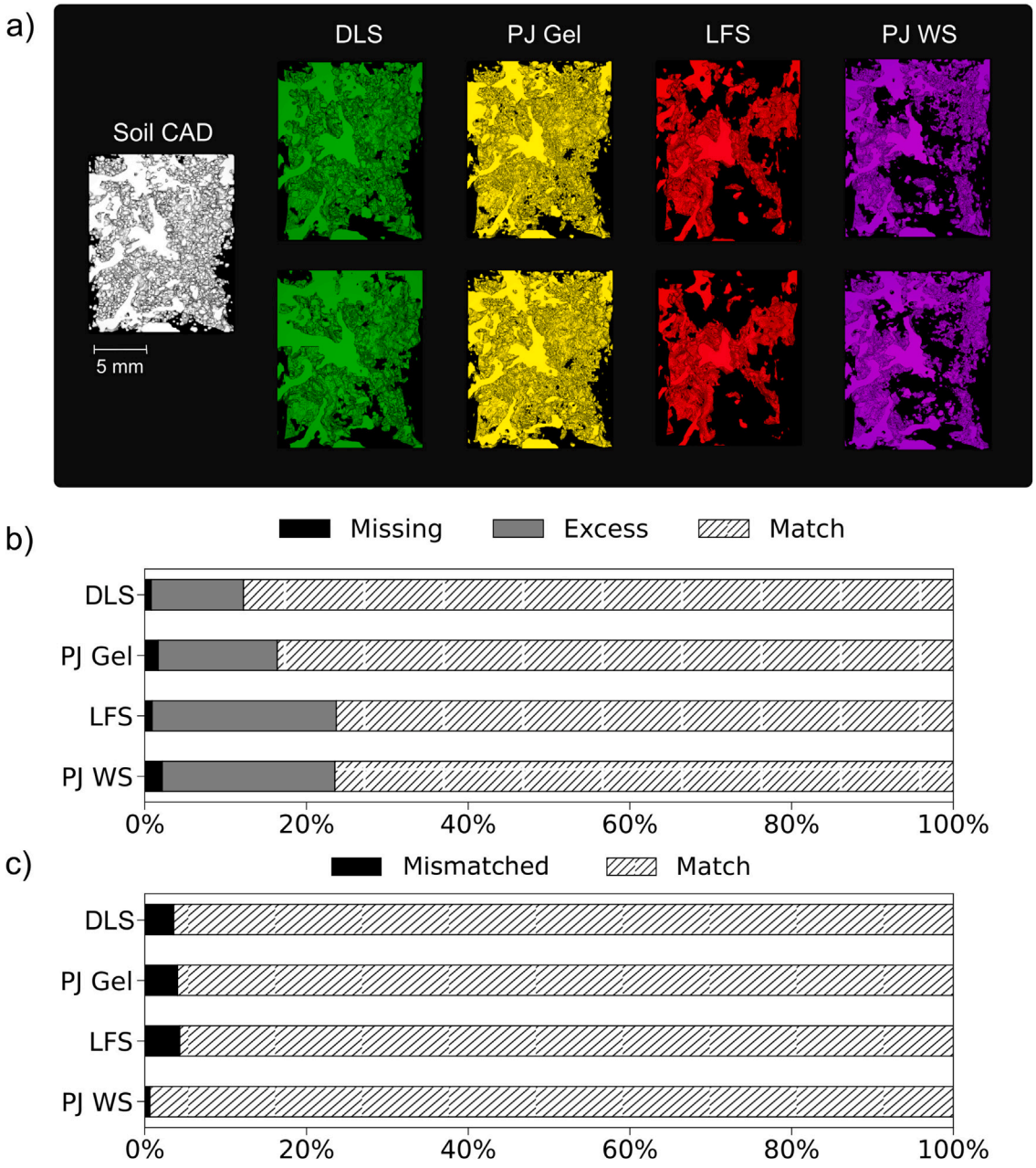

Fig. 1. Voxel-by-voxel analysis of 3D printed soil analogues. (a) 3D rendering of the pore space (i.e., negative of the 3D print) of the computer-aided design (CAD) and replicates of the four prints obtained with digital light synthesis (DLS), PolyJet with gel-based support material (PJ Gel), low-force stereolithography (LFS), and PolyJet with water-soluble support material (PJ WS). (b) Percentage of sample volume that is missing (CAD solid - print void), in excess (CAD void - print solid), or matching (CAD = print). (c) Percentage of sample volume that is mismatched or matching from replicate 3D prints for each technology.

the volume of the intruded fluid is then used to calculate the pore size distribution. To quantify the level of pore size distribution dissimilarity between the reference soil and the printed soils (for accuracy) or between multiple printed soils (for repeatability), we use the Earth Mover's Distance method (EMD), which provides a measure of the minimum amount of work required to change one distribution into the other (Rubner et al., 1998).

2.3.3. Wettability measurements and treatment:

Static water contact angles were measured to quantify the wettability of the printed analogues. Briefly, a 10 μL droplet of Milli-Q water was pipetted on a smooth, flat face of the printed analogues and its profile imaged after 10 s by a handheld digital microsope MicroDirect 1080P HDMI (Celestron). The images of the contact angle were then analyzed with Fiji with the drop shape analysis plugin Stalder et al. (2010).

To improve the wettability of the printed analogues, the samples were subjected to standard plasma cleaning for soft-lithography, which is traditionally used to impart hydrophilicity on Polydimethylsiloxane (PDMS) microfluidic reactors. First, the samples were thoroughly soaked in isopropanol to clean their surface from dust. Compressed air was then used to dry them out completely. Next, the samples were exposed to 1 min and then 2 min treatments by air plasma (Harrick Plasma, Inc. Ithaca, NY). Immediately following each treatment, the contact angle was measured on two different surfaces.

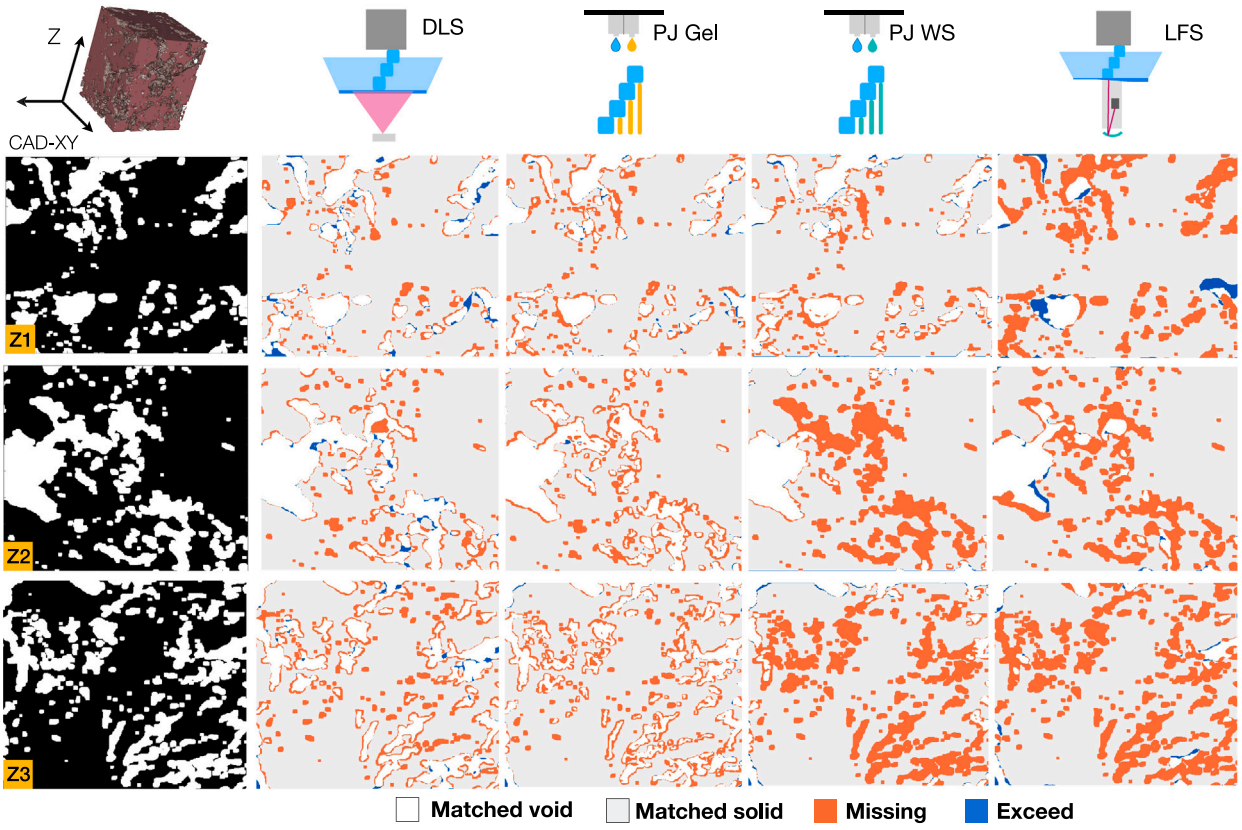

Fig. 2. Illustrative cross-sections at different z-depths of matched and mismatched pore geometry for each 3D printing technique tested. Left column shows a 3D rendering of the soil CAD and cross-sections with solid (black) and void (white). Additional columns show the corresponding cross-section produced by the four 3D printing technologies evaluated. The pore space is color-coded (corresponding to the summary of Fig. 1) for matched (gray), missing (orange), and excess (blue) volume. All cases lack the smallest pore features.

3. Results

The following section presents the results from all five quantitative metrics to assess accuracy and repeatability in all 3D printed technologies herein evaluated. The soil structure used here is considered to be a reasonable representation of "typical" soil characterized by its broad pore size distribution, multitude of interconnected pores, and intricate topology, as explicitly determined by Pérez-Reche et al. (2012).

3.1. Accuracy: similarity between printed analogues and reference soil

Qualitative comparison of pore structure: A visual inspection of the rendering of the original soil design and the porosity produced by the 3D printing techniques under evaluation is shown in Fig. 1a. The pore space of the soil CAD is shown in white, while the pore space of the printed soil analogue replicas are shown in different colors. Qualitatively, the soil CAD displays a complex structure with interconnected pores of diverse sizes that is most closely recreated by DLS (green) and PJ Gel (yellow) approaches. Analogues made by LFS (red) and PJ WS (magenta) lack much of the details of the pore structure by comparison.

Match/mismatch volume: Voxel-by-voxel comparisons of the soil CAD against the printed soil analogues are shown as stacked bar plots in Fig. 1b. *Missing* volume (shown as the black portion of the bar) represents portions of the solid that are missing in the printed soil (i.e., incorrect pores). Missing is consistently below 3% for all technologies, with even smaller percentages for DLS and LFS. One possible source for this structural error is infiltrated air bubbles during the drop injection process for traditional stereolithography, which can generate undesirable micropores in the final print (Patpatiya et al., 2022). Nevertheless, their contribution to printing errors is considerably low across all forms of 3D printing. *Excess* volume (shown as the gray portion of the bar) represents portions of the void that are missing in the printed soil (i.e., clogged pores). The percent of excess printed solid ranges from 11%–20%, with DLS at the lowest end. This structural defect can be attributed to printing error in the cases of DLS and LFS, and to incomplete removal of the support material in the cases of PJ Gel and PJ WS. *Match* volume (shown as the line shaded portion of the bar) represents portions of the sample (solid or void) that are correctly created in the printed soil. The percent of matched structure ranges from 75%–86%, with DLS and PJ Gel as the technologies that most closely resemble the CAD. Fig. 2 illustrates three cross-sections at different sample depths for each technique where details of the matched/missing/excess volume are indicated. In general, the image suggests that the smallest pore features are the hardest to reproduce for all printers. Overall, the outcomes of the voxel-by-voxel comparison are in agreement with the visual inspection of the 3D printed pore spaces (Fig. 1a). From the combined qualitative and quantitative analyses, the 3D printing techniques would rank as follows DLS > PJ Gel > LFS ~ PJ WS.

Permeability, specific surface area, connected porosity: Relative percent differences in permeability, SSA, and connected porosity between the CAD and each digitized print are reported in Fig. 3a (refer to the Table B.2 in the appendix for measured absolute values). In this analysis, properties reported from the soil CAD are taken as the reference point.

The simulated permeability of the soil CAD was found to be 8.62×10^{-10} m^2, which is within the upper range reported for typical Cambisol (Pawlowska and Pawlowski, 2014; Gonçalves-Maduro et al., 2020). All printed analogues had lower simulated permeability values than the CAD, with DLS differing by only −23.9%, while the other three techniques differed between −85.6 and −99.8% (see solid bars in Fig. 3a). Considering the importance of permeability for all hydrologic processes, DLS substantially outperforms the other approaches for the

porous structure here tested. Despite the substantial differences of the other printing techniques to recreate the desired permeability, fabricating realistic printed porous media analogues with permeabilities of $O(10^{-10})$ to $O(10^{-12})$ m^2 is already a great advance, bearing in mind previous studies of reported printed soil-like sample permeabilities in the range of 10^{-18} or 10^{-21} m^2 (Kong et al., 2019). While the analysis here presented is from image-based simulations, it permits an equitable comparison of the permeability of the soil and the prints at identical resolutions, which cannot be done with laboratory measurements because the soil sample no longer exists. Nevertheless, the interested reader is advised to work with cylindrical 3D prints (rather than the cubic samples here used) to create a proper seal at the interface between the printed analogue and the permeameter when applying fluid flow in the lab to measure permeability experimentally. It is recommended that the soil analogue and the flow through cell (if also 3D printed) are generated as independent pieces and assembled prior to experimentation and not printed as a single integrated unit. This will ensure maximal efficacy of the porous medium's post-processing (i.e., cleaning of the pores with water at high pressure), which is especially important for anisotropic samples.

The SSA of the soil CAD was found to be 5.69×10^3 m^{-1}. Most printed samples had lower SSA values than the CAD, with a narrow range of differences from −17.0% to −26.9%. Only PJ Gel produced a greater SSA of similar discrepancy magnitude (see dotted bars in Fig. 3a). This small difference suggests that SSA can be easily reproduced by 3D printing. Discrepancies of this structural property can be understood as the imbalance between reduced pore surface area, which results in lacking SSA, and the inevitable reduction in porosity, which leads to enlarged SSA during 3D printing.

The connected porosity of the soil CAD was estimated at 0.29. All printed samples exhibited lower connected porosity than the CAD, with variations between −32.4 to −80.3% (see stripped bars in Fig. 3a). For this structural property a clear trend emerges among the printing methods tested, where DLS shows the smallest discrepancy at −32.43%, followed by PJ Gel at −49.7%, then LFS with much greater difference at −71.09%, and PJ WS as the worst performer with −80.27% deviation. These quantitative results are consistent with the renderings in Fig. 1a, which illustrate that DLS most closely matches the desired porosity, while LFS and PJ WS exhibit the largest differences from the soil CAD.

The above comparative analysis of the pore structure between the prints and the soil CAD demonstrates that none of the 3D printing techniques can perfectly match the permeability, SSA, or connected porosity of the original design. However, the structural features that can be achieved are closer to a natural porous medium than a typical bead pack and are still useful for experimental work. Moreover, one 3D printing technique clearly outperforms the others in accuracy of these particular metrics. As such, ranking of the approaches from this analysis follows the order DLS ≫ PJ Gel ≥ LFS ∼ PJ WS.

Pore size distribution: The cumulative pore size distribution for the original soil CAD and the 1× magnification printed soil samples is presented in Fig. 4a. Consistently, the pores in the printed samples are larger than the original design, yet this shifted pore size is not sufficient to increase porosity as shown in Fig. 3a. The largest pore size in the soil CAD (gray line) was found to be ∼2400 μm, while the maximum pore size of all printed soils (colored lines) was larger (between ∼2700 μm and ∼3400 μm). The smallest pore size is dictated by the resolution of the soil scan (35 μm voxel size), which is comparable to the resolution of the printers (between 16 and 75 μm, as specified by the manufacturer). The soil CAD distribution increases most sharply between 244 μm and 944 μm (0.2 and 0.8 cumulative probability, respectively), indicating a large proportion of pores within this specific size range. The print distributions for all samples increase somewhat less sharply in this size range, except for prints made by PJ Gel. This suggests that a broader size distribution is typically produced with 3D printing of complex porous media. It is worth noting that only in samples from PJ Gel (yellow line), a substantial fraction of the pores (up to 0.6) tend to be smaller (<600 μm) than those of the CAD.

The distribution dissimilarity (through Earth Mover's Distance analysis) quantifies the absolute differences between the prints and the CAD distributions, as shown in Fig. 4b. As the figure shows, PJ Gel has the smallest dissimilarity from the CAD, followed closely by DLS and LFS. PJ WS had the largest dissimilarity. One important limitation of 3D printing analogues of geologic porous media is the difficulty in reproducing the smallest of pores, as is evident in the cumulative pore size distributions. On the one hand, for techniques that require support resin, the main challenge is removing this material from the smallest pores. On the other hand, support-free techniques are limited by both the resolution of the laser and the high viscosity of the resin that makes harder the removal process of the non-cured material. Successful cleaning of the pore space during post-processing is challenging, especially for complex geometries with structural features equal to or smaller than the printer resolution (Quan et al., 2020; Ye et al., 2024) (refer to Table 1 for details of the printers here used). Importantly, the technology that most closely recreated the CAD's pore size distribution was not the same as that which produced the closest permeability, SSA, and connected porosity. Thus, it is imperative that the user evaluates the trade-offs of matching the pore size distribution at the expense of properties like permeability. From a pore size distribution analysis, the ranking of the 3D printing technologies follows the order PJ Gel > DLS ∼ LFS ≫ PJ WS.

3.2. Repeatability: similarity between like-printed analogues

Qualitative comparison of pore structure: A visual evaluation of replicate pore structures pairs fabricated by the four 3D printing approaches is presented in Fig. 1a. Qualitatively, each soil analogue exceptionally resembles its replicate counterpart (compare pore structures of the same color top vs. bottom). While each printing type has obvious deficiencies in accurately recreating the soil CAD, the imperfections in each printing technique are very consistent. In the sample produced by DLS (green), only minor variations at the front boundary are apparent between the two replicates. Of note, is the upper left region, which is more connected for the bottom sample. This defect is in excess from the CAD and is here classified as a printing artifact. In addition, the bottom right corner for both replicates is similarly missing a small region of the pore space in the original design. This opening is missing from the CAD and can be considered to be a structural feature that is particularly difficult to recreate with DLS. The remaining details of the pore network are captured remarkably well in both prints. For the sample produced by PJ Gel (yellow), similar trends emerge: the upper left region has slight variations in connectivity between the two prints, and a small gap at the center of the sample shows up equally. Although samples made by LFS (red) and PJ WS (magenta) deviate the most from the soil CAD (e.g., final prints were unable to recover the dainty portions of the pore network), these techniques are still capable of duplicating the same imperfections from print to print. Thus, comparing replicate analogues (top and bottom) for the four additive manufacturing techniques under scrutiny demonstrates that whatever 3D printer is used will yield highly reproducible, albeit imperfect, soil analogues.

Match/mismatch volume: Voxel-by-voxel comparisons replicate pairs printed by the same technique are shown as stacked bar plots in Fig. 1c. Similar to the above section evaluating printing accuracy, here *mismatched* volume (shown as the black portion of the bar) indicates an inconsistent representation of the solid/void at identical locations of the replicate prints. That is, we group together missing/excess type errors since there is no reference structure. Mismatched volume is consistently below 5% for all approaches. *Match* volume (shown as the remaining line shaded portion of the bar) represents the proportion of the sample that is consistently classified (solid or pore) at identical locations of the replicate prints. The matched structure across replicates for all

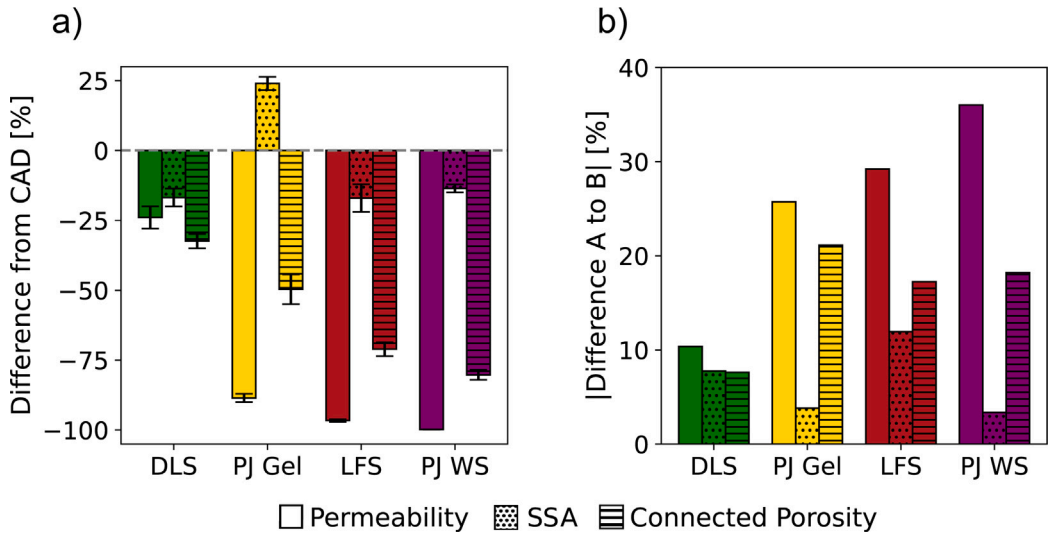

Fig. 3. Differences in permeability, specific surface area (SSA), and connected porosity between (a) the soil CAD and the printed soil analogues (accuracy) and (b) like-printed soil analogues (repeatability).

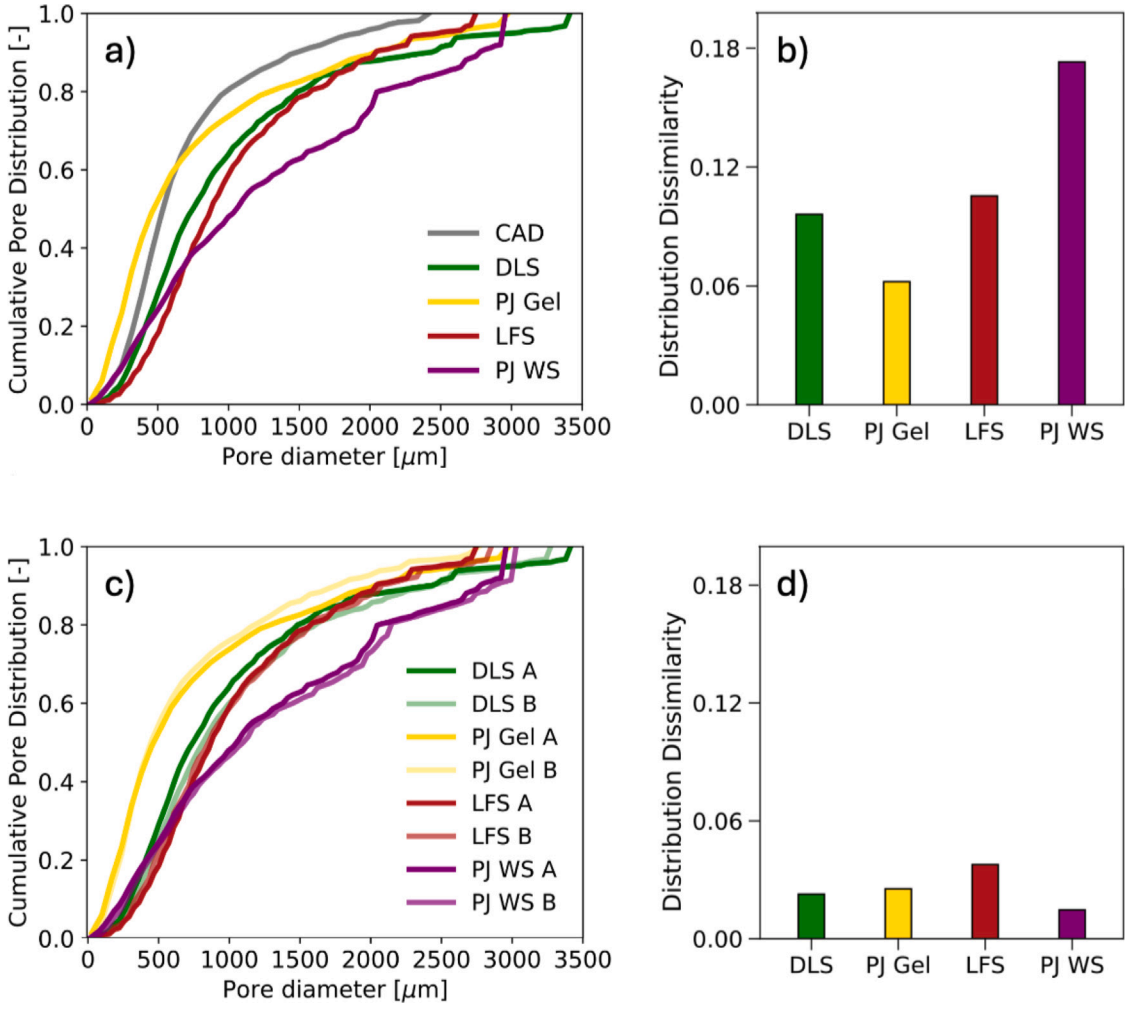

Fig. 4. (a) Cumulative pore size distribution and (b) their corresponding distribution dissimilarity metric for the soil CAD and all printed analogues (accuracy). (c) Cumulative pore size distribution and (d) their corresponding distribution dissimilarity metric for replicate analogue pairs (repeatability).

printing techniques is over 95%, a quantity that is in agreement with the rendering of the pore space shown in Fig. 1a. Of note, PJ WS exceeds the other three techniques in this evaluation with the lowest error (<1%) and greatest match (>99%) for replicate prints, but this trait should be taken into consideration with the other metrics herein presented when choosing a 3D printing technique.

Permeability, specific surface area, connected porosity: The differences in permeability, SSA, and connected porosity between replicate pairs printed by the same technique are reported in absolute percent in Fig. 3b. In terms of permeability (see solid bars in Fig. 3b), the choice of printing approach distinctly affects how similar this property will be for like-printed analogues. Our findings show that permeability differences among replicates range from 10% for DLS up to 36% for PJ WS. While the permeability differences for repeatability are important, they are considerably lower than those for accuracy. For SSA (see dotted bars in Fig. 3b), all printing approaches reproduce this property to a similar and faithful degree; differing by <11%. Our findings reveal that SSA is a structural feature that is the easiest to generate both accurately (as prescribed in the original design) and reproducibly across identical printed replicates. On the basis of connected porosity (see stripped bars in Fig. 3b), only DLS succeeded at matching this property closely between the two printed analogues (with the smallest difference of ~7%). All other printing approaches differed by ~20% in connected porosity. For pore networks that are structurally complex, it is crucial to identify the 3D printing approach that offers the closest corresponding permeability and connected porosity with each batch of prints. In this regard, DLS is the prominent performer for repeatability.

Pore size distribution: Pore size distributions of two replicate prints (A and B) are shown in Fig. 4c in dark/light coloring. Unfailingly, all four printing technologies under evaluation are capable of reproducing nearly identical pore size distributions in replicate analogues, for the given undisturbed soil design. This observation is quantitatively confirmed by the distribution dissimilarity analysis for like-fabricated analogues, which is very low (<0.04) across the board for all technologies (see Fig. 4d). This crucial finding demonstrates that, even when one of the evaluated 3D printing techniques falls short to accurately recreate the pore size distribution of the CAD, any imperfections in the pore network will be rendered in near identical ways for every print.

3.3. Surface wettability

3D printing resins are strongly hydrophobic, producing water contact angles > 86° (see Fig. 5 circles). Through this measurement, is it evident that contact angle variability is substantial among all printing techniques, with PJ WS being the most erratic. Plasma treatment is traditionally used to render polymer substrates temporarily water wet. Here, we expose our 3D printed soil analogues to air plasma as per standard soft-lithography protocols because it is an approach to modify the surface wettability of substrates that does not suffer from the mass diffusion limitations of liquid silanization. Two tests were conducted to understand how the plasma exposure influences the wettability of the resin prints. The first treatment (1 min plasma exposure) diminished the contact angle for all samples to span a range of 30–66° (see Fig. 5 triangles). The second treatment (2 min plasma exposure) produced mixed results in improved wettability, whereby one resin became more wettable (DLS), some resins stayed similarly wettable (PJ Gel and LFS), and another became slightly less wettable (PJ WS) (see Fig. 5 diamonds). Such a reversion to hydrophobic surfaces is not uncommon with plasma treatment and must be fine-tuned for each resin type. In general, for 3D printed soil analogues we recommend the shorter plasma treatment which guarantees an improved wettability, even if the contact angle is at an intermediate value (30–60°) of the normal reported range in real soils (0–120°) (Morales et al., 2010; Woche et al., 2005; Bachmann et al., 2000a,b; Leelamanie and Karube, 2013). Because the longest distance to permeate plasma into the pore space from any external sample surface is short (here, ~5 mm), we expect that this treatment improves the wettability of the pores inside the sample in a similar way as the sample's measured exterior. Verifying wettability changes to the internal pore network surface, however, is beyond the scope of this work.

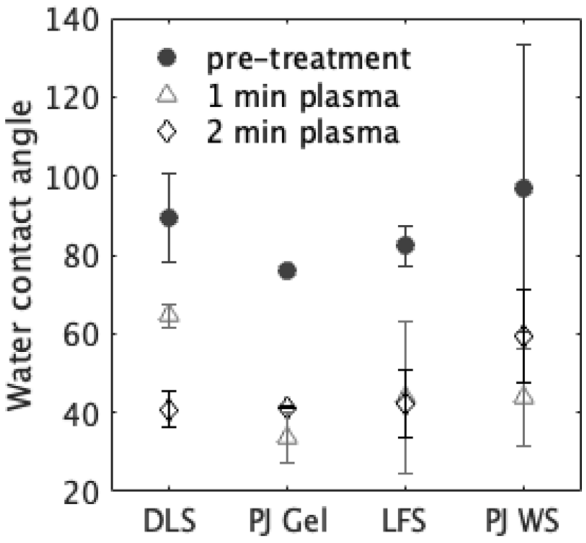

Fig. 5. Water contact angle measurements of printed samples prior to and post plasma treatment (1 and 2 min) to improve their wettability.

4. Discussion

4.1. Recommendations for best 3D printing with maximal accuracy and repeatability

While each soil structure is one of a kind, we are confident that the recommendations made here for soil/rock analogue fabrication with 3D printing will hold for other complex porous media. The authors invite the readership to contribute to expand the assessment of accuracy and repeatability of any of the 3D printing approaches here presented (with priority placed on DLS) for alternative soil structures.

The thorough evaluation here presented reveals that the best printing technology to fabricate soil analogues that accurately capture the pore structural complexity of real soils/rocks is plainly DLS. This approach dominantly outperformed the others in terms of accuracy for most similar by visual inspection, greatest voxel-by-voxel match, and least difference in permeability, SSA, and connected porosity from the CAD. Although pore size distribution was best captured by PJ Gel, DLS came in at a close second for this criterion. All three other approaches performed similarly worse, especially in terms of permeability and connected porosity, which are at the center of all hydrologic processes that these analogues would be used for studying. Both PolyJet-based technologies had pore clogging issues that affected the quality of the prints. Our analysis suggests that gel (SUP705) is more easily removed than water soluble (SUP706) support material in intricate pore networks like the soil one here tested. Attempts to artificially boost the pore space accuracy by increasing the sample's printing magnification did not sufficiently improve the recovered pore features to achieve better results than DLS, which has excellent performance at the original 1:1 scale.

Parallel evaluation for the best printing technology to fabricate identical soil analogues indicates that all considered approaches are very good for replication, with a moderately better performance by DLS over the rest. Replicates made by the same approach are alike in visual similarity, resemble one another in high voxel-by-voxel match, and show nearly identical matches in pore size distribution. The largest difference between the four tested technologies is seen in the absolute difference in permeability, SSA, and connected porosity for which DLS produces prints that are objectively almost exactly the same. For all technologies, no clear issues emerged in reproducing the same imperfect pore structure from one printing batch to the next. With the exception of DLS, all analogues were produced and post-processed in back to back batches. The samples from DLS were produced by two

different providers (UC Davis TEAM and Diversified Plastics) with a time gap of two years, which is a further testament to this technique's exceptional repeatability. This suggests that whatever difficulties exist during the printing process and sample post-processing (e.g., removing the support material), the final outcome is a nearly identical copy from print to print. Moving forward, the authors encourage future 3D printing users to adopt the quality control metrics herein proposed to better cross evaluate 3D printing approaches with other pore network samples.

4.2. Limitations and remaining qualities to optimize for 3D printing geologic porous media

The latest advances in high-resolution 3D printing are finally capable of reproducing key characteristics of porous media, including geometry, permeability, specific surface area, porosity, and pore size distribution *at the original size* with a single material in a repeatable manner. Wettability and surface texture, however, are geologic properties that cannot yet be perfectly matched in addition to the above listed physical features. Resin-based printers can accurately fabricate the pore geometry, but the wettability is different (even after plasma treatment) from what might be expected of natural porous media (Ishutov et al., 2021; Bacher et al., 2015; Otten et al., 2012; Suzuki et al., 2017; Dal Ferro and Morari, 2015). Powder-printing technologies enable the fabrication of 3D prints with surface texture and wettability that can more closely resemble soils and rocks, but the geometry of pore systems is poorly replicated (Ishutov et al., 2021; Anjikar et al., 2020; Ferrari et al., 2022; Song et al., 2020). Nevertheless, for research that requires fabrication of identical copies of a natural pore structure, functionality and accuracy are paramount, even if they lack certain surface properties.

The workflow herein presented can be applied to replicate the physical micro heterogeneity of permeable soils and rocks within the dimensional limit of resin-based printers. Improvements made to the wettability of the soil analogues show that this surface property can be adjusted through plasma treatment to closely approach measurements from real soils, which the literature reports span between 0–120° (Morales et al., 2010; Woche et al., 2005; Bachmann et al., 2000a,b; Leelamanie and Karube, 2013). Yet, the longevity of its effect and its efficacy to uniformly increase the wettability of the entire pore network must still be evaluated in greater detail. Nanoporosity can be introduced by use of powder-based printers at the expense of reproducing the intricate microstructure blueprinted in the CAD.

The authors recommend that 3D printed geologic analogues for applications in fluid flow should choose an optimal size and resolution of the printed samples by "reverse engineering" the system. This implies selecting the smallest physical size of the analogue that can be used for laboratory experimentation (e.g., minimum 10 mm diameter × 20 mm length), using this sample size to obtain the maximum image resolution of the original sample, and selecting a 3D printer whose accuracy and resolution can support the detail required. Omission of these three considerations may render a sample that is too small for fluid flow experimentation, or a microstructure that is unrecognizable by the imaging technique or unprintable at the original scale. The authors note that the sample herein analyzed is dominated by large pores (≥500 μm), which contain a pore size that is suitable to the printer resolution. The applicability of this method to soils with pores dominated by even finer textured grains requires reviewing the resolution of the image of the original soil sample and the printer resolution to ensure the finest details are both visible for CAD construction and printable in the final product.

5. Summary and conclusions

In this work we present one of the most detailed descriptions and measurements of structural and hydrologic properties in 3D printed heterogeneous porous media. In doing so, we shed light on the quality of 3D printing to produce identical soil/rock analogues, which has been an elusively revolutionary technique for investigating subsurface processes due largely to the improper removal of support material from the pore space, a longstanding bottleneck. We have surveyed the capability of four different 3D printing technologies for producing soil analogues through direct comparison of microtomography imaging of their pore space. Typical metrics were used for quantifying the recovered pore morphology to evaluate how well each technique can relate their print to the complex soil design they were crafted from (accuracy), as well as how close the prints are to one another (repeatability). One particular technology emerged as the best–DLS. No trade-off was required between accuracy and repeatability.

Strategies to overcome accuracy limitations are unique to each printing strategy here investigated. Generally, we recommend avoiding approaches that require the use of support material in the voids during fabrication (PolyJet) because its removal from intricate pore networks is notoriously difficult. For LFS, tilting the sample by 45° on edge or corner during printing greatly and similarly improved the final product. To alleviate the extreme hydrophobicity of resin printing, we propose plasma treatment. While some limitations remain to be resolved (e.g., printing the smallest of pores and treating the polymer surface to change its wettability and surface texture), we are optimistic that the soil/environmental science community could be on the verge of moving past using glass beads and sand for performing controlled transport experiments in the laboratory. The adoption of a new generation of model porous media with realistic pore structures can take advantage of the large databases of microtomography images of undisturbed soils/rocks representative of myriad systems, land uses, and applications. High quality 3D printed soil/rock analogues can open up many yet unexplored opportunities to investigate the impacts of pore structural characteristics on flow, transport, and reactions in environmentally relevant media.

CRediT authorship contribution statement

Janis E. Patiño: Writing – review & editing, Writing – original draft, Methodology, Investigation, Formal analysis, Conceptualization. **Filippo Miele:** Writing – review & editing, Methodology, Formal analysis, Data curation. **Alejandro J. Perez:** Methodology, Formal analysis. **Zoe Kanavas:** Formal analysis, Data curation. **Mackenzie L. Dughi:** Methodology, Data curation. **Verónica L. Morales:** Writing – review & editing, Writing – original draft, Validation, Supervision, Resources, Project administration, Methodology, Investigation, Funding acquisition, Formal analysis, Data curation, Conceptualization.

Declaration of competing interest

The authors declare that they have no known competing financial interests or personal relationships that could have appeared to influence the work reported in this paper.

Data availability

Data will be made available on request.

Acknowledgments

Acknowledgment is made to the U.S. NSF (EAR-1847689, EAR-2345366), the Engineering Research Center Program of NSF under Cooperative Agreement, United States (EEC-1449501), BARD fund, United States (IS-5694-24), and the CAMPOS Jump Start Grant, United States. F.M. gratefully acknowledges the financial support from the Swiss National Science Foundation - Postdoc Mobility Fellowship, Switzerland (SNF, grant Nr. P2LAP2_199473). The authors also thank Drs Sergey Ishutov and Johannes Koestel for fruitful discussions on 3D printing, Dr Erkin Seker and Ms Eleanor Fadely for guidance on plasma treatment, Steven Lucero for the CAD design and technical support, as well as the editor and anonymous reviewers for their feedback.

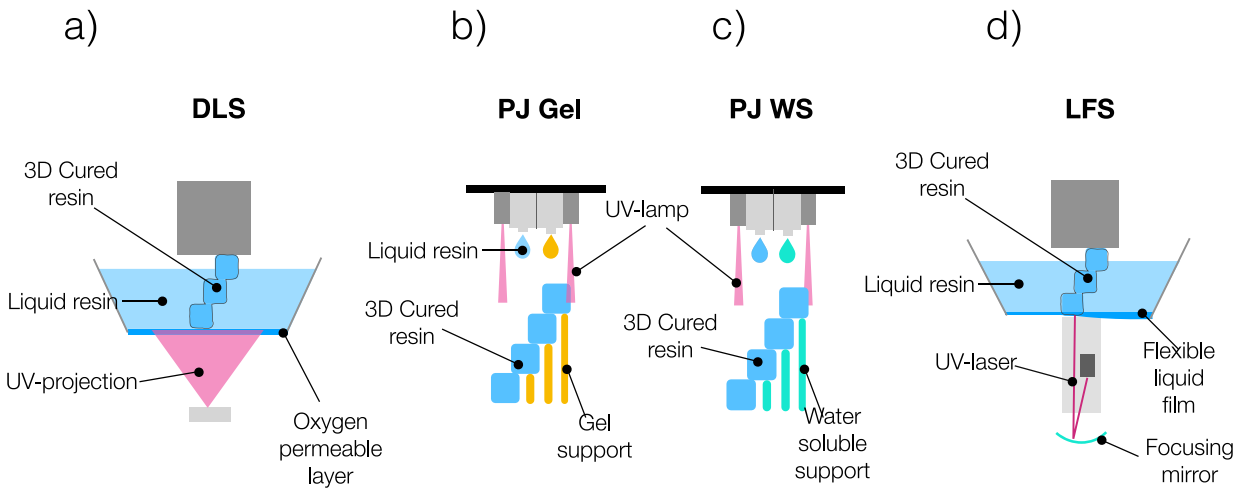

Fig. A.6. Schematic of the printing mechanism for the four 3D printers technologies investigated. (a) Digital Light Synthesis (DLS). (b) UV curing of photopolymers by PolyGet and subsequent removal of the Gel or (c) Water support, WS. (d) Low Force Stereolithography (LFS).

Fig. A.7. Photograph of the produced printed soil analogues by DLS, PJ Gel, PJ WS, and LFS arranged left to right.

Appendix A. Summary of 3D printed technologies tested

DLS 3D printing builds on principles of stereolithography (SLA). Both DLS and SLA use UV light (laser spot and projector, respectively) to cure liquid resin into solid material. Briefly, the DLS printing process works by holding a thin layer of uncured liquid resin in a transparent tank, which is subsequently cured into a specific pattern with a UV laser source from below. An oxygen permeable layer at the base of the tank ensures the UV light penetrates only the first 70 μm of the tank. The printed prototype is attached to a building platform that is raised incrementally as the printing process progresses. In doing so, the technique forgoes the need to use support material to prop the voids open because it works with gravity to create the print. Recurrently, the transparent tank is refilled with more liquid resin, a new pattern layer is cured with UV light, and the 3D print is extracted from above (see Fig. A.6a). The digital light projector (as opposed to a laser) allows the entire cross-section of the print to be cured with a single pass. This process results in printing times that are up to 10 × faster than traditional SLA printers, because the laser spot has to scan the entire cross-section (DiversifiedPlastics, 2024, 2023).

PolyJet 3D printing works by jetting droplets of liquid photopolymer onto a build platform, one layer at a time. Each droplet is cured by a point-wise UV light source, hardening it into place. The process is repeated until the entire model is built. Support material is injected into positions where voids should be located, providing subsequent layers with supporting forces. Indeed, this support material helps to keep the model in place during printing and prevents it from collapsing. After printing, the support material must be removed by post-processing by means of high-pressure air or water flushing, vapor steaming, or oven drying (Dal Ferro and Morari, 2015).

LFS 3D printing is also a derivative of SLA, but an intermediate with DLS. For this technique, the standard SLA technique is improved by (1) the use of a flexible resin tank that reduces the peeling forces in the cleaning step, (2) a point-by-point surface's orthogonal laser's spot that reduces unwanted lateral laser curing, and (3) a smaller laser spot size (FormLabs, 2019) (see Fig. A.7).

Appendix B. Measured permeability, specific surface area, connected porosity

See Fig. B.8 and Table B.2.

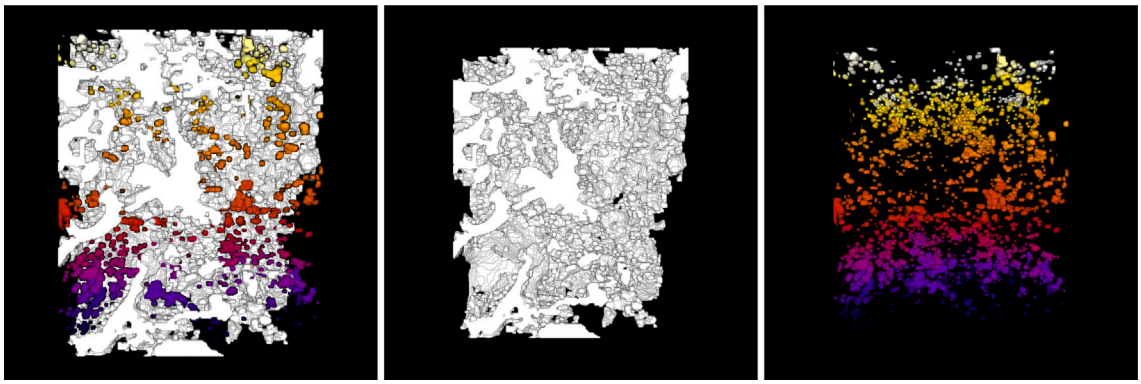

Fig. B.8. Identification of percolating and isolated pores from microtomography images of a soil pore network using Particle Analyzer (FIJI). (Left) shows all individual pores in the sample. (Center) shows only the percolating pore connecting top to bottom boundaries. (Right) shows only isolated pores.

Table B.2
Transport properties for CAD and printed samples obtained from image analysis and flow simulations.

Label	Scale	Permeability [m^2]	Specific surface area [$\times 10^3$ m^{-1}]	Connected porosity [–]
CAD	–	8.62×10^{-10}	5.686	0.290
DLS A	1x	6.56×10^{-10}	4.714	0.196
DLS B	1x	5.88×10^{-10}	5.086	0.181
PJ Gel A	1x	9.89×10^{-11}	7.057	0.146
PJ Gel B	1.5x	1.24×10^{-10}	6.771	0.177
LFS A	1x	2.91×10^{-11}	4.714	0.084
LFS B	1x	2.06×10^{-11}	4.143	0.069
PJ WS A	1x	1.56×10^{-12}	4.814	0.057
PJ WS B	1.5x	2.13×10^{-12}	5.086	0.068

References

Anjikar, Ishan S., Wales, Shelby, Beckingham, Lauren E., 2020. Fused filament fabrication 3-D printing of reactive porous media. Geophys. Res. Lett. 47 (9), e2020GL087665.

Anna, Pietro de, Jimenez-Martinez, Joaquin, Tabuteau, Hervé, Turuban, Regis, Le Borgne, Tanguy, Derrien, Morgane, Méheust, Yves, 2014. Mixing and reaction kinetics in porous media: An experimental pore scale quantification. Environ. Sci. Technol. 48 (1), 508–516.

Arrieta-Escobar, Javier A., Derrien, Delphine, Ouvrard, Stéphanie, Asadollahi-Yazdi, Elnaz, Hassan, Alaa, Boly, Vincent, Tinet, Anne-Julie, Dignac, Marie-France, 2020. 3D printing: An emerging opportunity for soil science. Geoderma 378, 114588.

Bacha, Tristan W., Manuguerra, Dylan C., Marano, Robert A., Stanzione, Joseph F., 2021. Hydrophilic modification of SLA 3D printed droplet generators by photochemical grafting. RSC Adv. 11 (35), 21745–21753.

Bacher, Matthias, Schwen, Andreas, Koestel, John, 2015. Three-dimensional printing of macropore networks of an undisturbed soil sample. Vadose Zone J. 14 (2), vzj2014–08.

Bachmann, Joerg, Ellies, A., Hartge, K.H., 2000a. Development and application of a new sessile drop contact angle method to assess soil water repellency. J. Hydrol. 231, 66–75.

Bachmann, J., Horton, R., Van Der Ploeg, R.R., Woche, S., 2000b. Modified sessile drop method for assessing initial soil–water contact angle of sandy soil. Soil Sci. Soc. Am. J. 64 (2), 564–567.

Bandara, Uditha C., Tartakovsky, Alexandre M., Palmer, Bruce J., 2011. Pore-scale study of capillary trapping mechanism during CO2 injection in geological formations. Int. J. Greenh. Gas Control (ISSN: 17505836) 5 (6), 1566–1577. http://dx.doi.org/10.1016/j.ijggc.2011.08.014, URL https://linkinghub.elsevier.com/retrieve/pii/S1750583611001708.

Benzhong, Zhao, Christopher, W. MacMinn, Bauyrzhan, K. Primkulov, Yu, Chen, Albert, J. Valocchi, Jianlin, Zhao, Qinjun, Kang, Kelsey, Bruning, James, E. McClure, Cass, T. Miller, Abbas, Fakhari, Diogo, Bolster, Thomas, Hiller, Martin, Brinkmann, Luis, Cueto-Felgueroso, Daniel, A. Cogswell, Rahul, Verma, Maša, Prodanović, Julien, Maes, Sebastian, Geiger, Morten, Vassvik, Alex, Hansen, Enrico, Segre, Ran, Holtzman, Zhibing, Yang, Chao, Yuan, Bruno, Chareyre, Ruben, Juanes, 2019. Comprehensive comparison of pore-scale models for multiphase flow in porous media. Proc. Natl. Acad. Sci. 116 (28), 13799–13806. http://dx.doi.org/10.1073/pnas.1901619116, arXiv:https://www.pnas.org/doi/pdf/10.1073/pnas.1901619116, URL https://www.pnas.org/doi/abs/10.1073/pnas.1901619116.

Berkowitz, Brian, Scher, Harvey, Silliman, Stephen E., 2000. Anomalous transport in laboratory-scale, heterogeneous porous media. Water Resour. Res. 36 (1), 149–158. http://dx.doi.org/10.1029/1999WR900295, arXiv:https://agupubs.onlinelibrary.wiley.com/doi/pdf/10.1029/1999WR900295, URL https://agupubs.onlinelibrary.wiley.com/doi/abs/10.1029/1999WR900295.

Blunt, Martin J, Bijeljic, Branko, Dong, Hu, Gharbi, Oussama, Iglauer, Stefan, Mostaghimi, Peyman, Paluszny, Adriana, Pentland, Christopher, 2013. Pore-scale imaging and modelling. Adv. Water Resour. 51, 197–216.

Bordoloi, Ankur Deep, Scheidweiler, David, Dentz, Marco, Bouabdellaoui, Mohammed, Abbarchi, Marco, De Anna, Pietro, 2022. Structure induced laminar vortices control anomalous dispersion in porous media. Nature Commun. (ISSN: 2041-1723) 13 (1), 3820. http://dx.doi.org/10.1038/s41467-022-31552-5, URL https://www.nature.com/articles/s41467-022-31552-5.

Briggs, Martin A., Day-Lewis, Frederick D., Zarnetske, Jay P., Harvey, Judson W., 2015. A physical explanation for the development of redox microzones in hyporheic flow. Geophys. Res. Lett. 42 (11), 4402–4410. http://dx.doi.org/10.1002/2015GL064200, arXiv:https://agupubs.onlinelibrary.wiley.com/doi/pdf/10.1002/2015GL064200, URL https://agupubs.onlinelibrary.wiley.com/doi/abs/10.1002/2015GL064200.

Brouwer, C., Prins, K., Kay, M., Heibloem, M., 1988. Irrigation water management: irrigation methods. Train. Man. 9 (5), 5–7.

Bultreys, Tom, De Boever, Wesley, Cnudde, Veerle, 2016. Imaging and image-based fluid transport modeling at the pore scale in geological materials: A practical introduction to the current state-of-the-art. Earth-Sci. Rev. 155, 93–128.

Catterton, Megan A., Montalbine, Alyssa N., Pompano, Rebecca R., 2021. Selective fluorination of the surface of polymeric materials after stereolithography 3D printing. Langmuir 37 (24), 7341–7348.

Dal Ferro, Nicola, Morari, F., 2015. From real soils to 3D-printed soils: Reproduction of complex pore network at the real size in a silty-loam soil. Soil Sci. Soc. Am. J. 79 (4), 1008–1017.

DiversifiedPlastics, 2023. Design and Manufacture the Impossible. Technical Report, Diversified Plastics Inc.

DiversifiedPlastics, 2024. Faster Manufacturing for Go-To-Market Success. Technical Report, Diversified Plastics Inc.

Domander, Richard, Felder, Alessandro A., Doube, Michael, 2021a. BoneJ2 - refactoring established research software. Wellcome Open Res. (ISSN: 2398-502X) 6, 37. http://dx.doi.org/10.12688/wellcomeopenres.16619.2, URL https://wellcomeopenresearch.org/articles/6-37/v2.

Domander, Richard, Felder, Alessandro A., Doube, Michael, 2021b. BoneJ2-refactoring established research software. Wellcome Open Res. 6.

Ferrari, Andrea, Jimenez-Martinez, Joaquin, Borgne, Tanguy Le, Méheust, Yves, Lunati, Ivan, 2015. Challenges in modeling unstable two-phase flow experiments in porous micromodels. Water Resour. Res. 51 (3), 1381–1400.

Ferrari, Alessio, Rosone, Marco, La Rosa, Silvia, Sapienza, Giovanni, 2022. Microstructural characterization of a 3D-printed soil. Soils Rocks 45.

FormLabs, 2019. 4 Ways LFS 3D Printing Produces Better Parts. Technical Report, formlabs.

Gonçalves-Maduro, Letícia, Armindo, Robson André, Turek, Maria Eliza, Wendroth, Ole, 2020. Soil water and fuel permeability of a cambisol in southern Brazil and its spatial behavior: A case study. Vadose Zone J. 19 (1), e20035.

Gramling, Carolyn M., Harvey, Charles F., Meigs, Lucy C., 2002. Reactive transport in porous media: a comparison of model prediction with laboratory visualization. Environ. Sci. Technol. (ISSN: 0013-936X) 36 (11), 2508–2514. http://dx.doi.org/10.1021/es0157144, Publisher: American Chemical Society.

Heyman, Joris, Lester, Daniel R., Turuban, Règis, Le Borgne, Tanguy, 2020. Stretching and folding sustain microscale chemical gradients in porous media. Proc. Natl. Acad. Sci. 117, 13359–13365.

Hilden, J., Linden, S., Planas, B., 2019. User Guide GeoDict Release 2020. Math2Market GmbH.

Hodder, Kevin J., Nychka, John A., 2019. Silane treatment of 3D-printed sandstone models for improved spontaneous imbibition of water. Transp. Porous Media 129 (2), 583–598.

Huang, Pan Ming, Li, Yuncong, Sumner, Malcolm E., 2011. Handbook of Soil Sciences: Resource Management and Environmental Impacts. CRC Press.

Ishutov, Sergey, Hasiuk, Franciszek J, Harding, Chris, Gray, Joseph N, 2015. 3D printing sandstone porosity models. Interpretation 3 (3), SX49–SX61.

Ishutov, Sergey, Hasiuk, Franciszek J., Jobe, Dawn, Agar, Susan, 2018a. Using resin-based 3D printing to build geometrically accurate proxies of porous sedimentary rocks. Groundwater 56 (3), 482–490.

Ishutov, Sergey, Hodder, Kevin, Chalaturnyk, Rick, Zambrano-Narvaez, Gonzalo, 2021. Replication of carbonate reservoir pores at the original size using 3D printing. Petrophysics 62 (05), 477–485.

Ishutov, Sergey, Jobe, T. Dawn, Zhang, Shuo, Gonzalez, Miguel, Agar, Susan M., Hasiuk, Franciszek J., Watson, Francesca, Geiger, Sebastian, Mackay, Eric, Chalaturnyk, Richard, 2018b. Three-dimensional printing for geoscience: Fundamental research, education, and applications for the petroleum industry. AAPG Bull. 102 (1), 1–26.

Kafle, Abishek, Luis, Eric, Silwal, Raman, Pan, Houwen Matthew, Shrestha, Pratisthit Lal, Bastola, Anil Kumar, 2021. 3D/4D printing of polymers: Fused deposition modelling (FDM), selective laser sintering (SLS), and stereolithography (SLA). Polymers 13 (18), 3101.

Kang, Peter K., de Anna, Pietro, Nunes, Joao P., Bijeljic, Branko, Blunt, Martin J., Juanes, Ruben, 2014. Pore-scale intermittent velocity structure underpinning anomalous transport through 3-D porous media. Geophys. Res. Lett. 41 (17), 6184–6190. http://dx.doi.org/10.1002/2014GL061475, arXiv:https://agupubs.onlinelibrary.wiley.com/doi/pdf/10.1002/2014GL061475, URL https://agupubs.onlinelibrary.wiley.com/doi/abs/10.1002/2014GL061475.

Kong, Lingyun, Ostadhassan, Mehdi, Liu, Bo, Li, Chunxiao, Liu, Kouqi, 2019. Multifractal characteristics of MIP-based pore size distribution of 3D-printed powder-based rocks: a study of post-processing effect. Transp. Porous Media 129, 599–618.

Kurz, Dorothee L., Secchi, Eleonora, Carrillo, Francisco J., Bourg, Ian C., Stocker, Roman, Jimenez-Martinez, Joaquin, 2022. Competition between growth and shear stress drives intermittency in preferential flow paths in porous medium biofilms. Proc. Natl. Acad. Sci. 119 (30), e2122202119. http://dx.doi.org/10.1073/pnas.2122202119

Leelamanie, D.A.L., Karube, Jutaro, 2013. Soil-water contact angle as affected by the aqueous electrolyte concentration. Soil Sci. Plant Nutr. 59 (4), 501–508.

Meakin, Paul, Tartakovsky, Alexandre M., 2009. Modeling and simulation of pore-scale multiphase fluid flow and reactive transport in fractured and porous media. Rev. Geophys. 47 (3), http://dx.doi.org/10.1029/2008RG000263, arXiv:https://agupubs.onlinelibrary.wiley.com/doi/pdf/10.1029/2008RG000263, URL https://agupubs.onlinelibrary.wiley.com/doi/abs/10.1029/2008RG000263.

Meyer, Daniel W., Bijeljic, Branko, 2016. Pore-scale dispersion: Bridging the gap between microscopic pore structure and the emerging macroscopic transport behavior. Phys. Rev. E 94 (1), 013107.

Morales, Veronica L., Dentz, Marco, Willmann, Matthias, Holzner, Markus, 2017. Stochastic dynamics of intermittent pore-scale particle motion in three-dimensional porous media: Experiments and theory. Geophys. Res. Lett. 44 (18), 9361–9371.

Morales, Verónica L., Parlange, J.-Yves, Steenhuis, Tammo S., 2010. Are preferential flow paths perpetuated by microbial activity in the soil matrix? A review. J. Hydrol. 393 (1–2), 29–36.

Muljadi, Bagus P., Blunt, Martin J., Raeini, Ali Q., Bijeljic, Branko, 2016. The impact of porous media heterogeneity on non-Darcy flow behaviour from pore-scale simulation. Adv. Water Resour. (ISSN: 03091708) 95, 329–340. http://dx.doi.org/10.1016/j.advwatres.2015.05.019, URL https://linkinghub.elsevier.com/retrieve/pii/S030917081500113X.

Otten, Wilfred, Pajor, Radoslaw, Schmidt, Sonja, Baveye, Philippe C., Hague, R., Falconer, Ruth E., 2012. Combining X-ray CT and 3D printing technology to produce microcosms with replicable, complex pore geometries. Soil Biol. Biochem. 51, 53–55.

Patpatiya, Parth, Chaudhary, Kailash, Shastri, Anshuman, Sharma, Shailly, 2022. A review on polyjet 3D printing of polymers and multi-material structures. Proc. Inst. Mech. Eng. C 236 (14), 7899–7926.

Pawlowska, Malgorzata, Pawlowski, Lucjan, 2014. Management of Pollutant Emission from Landfills and Sludge. CRC Press.

Pereira Nunes, J.P., Blunt, M.J., Bijeljic, B., 2016. Pore-scale simulation of carbonate dissolution in micro-CT images. J. Geophys. Res. Solid Earth 121 (2), 558–576. http://dx.doi.org/10.1002/2015JB012117, arXiv:https://agupubs.onlinelibrary.wiley.com/doi/pdf/10.1002/2015JB012117, URL https://agupubs.onlinelibrary.wiley.com/doi/abs/10.1002/2015JB012117.

Pérez-Reche, F.J., Taraskin, S.N., Otten, W., Viana, M.P., Costa, L. Da F., Gilligan, C.A., 2012. Prominent effect of soil network heterogeneity on microbial invasion. Phys. Rev. Lett. 109 (9), 098102. http://dx.doi.org/10.1103/PhysRevLett.109.098102 (ISSN 0031-9007, 1079-7114), URL https://link.aps.org/doi/10.1103/PhysRevLett.109.098102.

Quan, Haoyuan, Zhang, Ting, Xu, Hang, Luo, Shen, Nie, Jun, Zhu, Xiaoqun, 2020. Photo-curing 3D printing technique and its challenges. Bioact. Mater. (ISSN: 2452199X) 5 (1), 110–115. http://dx.doi.org/10.1016/j.bioactmat.2019.12.003, URL https://linkinghub.elsevier.com/retrieve/pii/S2452199X19300714.

Rubner, Y., Tomasi, C., Guibas, L.J., 1998. A metric for distributions with applications to image databases. In: Sixth International Conference on Computer Vision (IEEE Cat. No.98CH36271). Narosa Publishing House, Bombay, India, ISBN: 978-81-7319-221-0, pp. 59–66. http://dx.doi.org/10.1109/ICCV.1998.710701, URL http://ieeexplore.ieee.org/document/710701/.

Scheidweiler, David, Miele, Filippo, Peter, Hannes, Battin, Tom J, de Anna, Pietro, 2020. Trait-specific dispersal of bacteria in heterogeneous porous environments: from pore to porous medium scale. J. R. Soc. Interface 17 (164), 20200046.

Schindelin, Johannes, Arganda-Carreras, Ignacio, Frise, Erwin, Kaynig, Verena, Longair, Mark, Pietzsch, Tobias, Preibisch, Stephan, Rueden, Curtis, Saalfeld, Stephan, Schmid, Benjamin, Tinevez, Jean-Yves, White, Daniel James, Hartenstein, Volker, Eliceiri, Kevin, Tomancak, Pavel, Cardona, Albert, 2012. Fiji: an open-source platform for biological-image analysis. Nat. Methods 9 (7), 676–682. http://dx.doi.org/10.1038/nmeth.2019 (ISSN 1548-7091, 1548-7105), URL https://www.nature.com/articles/nmeth.2019.

Sirivithayapakorn, Sanya, Keller, Arturo, 2003. Transport of colloids in saturated porous media: A pore-scale observation of the size exclusion effect and colloid acceleration. Water Resour. Res. 39 (4).

Sole-Mari, Guillem, Fernàndez-Garcia, Daniel, Sanchez-Vila, Xavier, Bolster, Diogo, 2020. Lagrangian modeling of mixing-limited reactive transport in porous media: Multirate interaction by exchange with the mean. Water Resour. Res. 56 (8), http://dx.doi.org/10.1029/2019WR026993, e2019WR026993, arXiv:https://agupubs.onlinelibrary.wiley.com/doi/pdf/10.1029/2019WR026993, URL https://agupubs.onlinelibrary.wiley.com/doi/abs/10.1029/2019WR026993.

Song, Rui, Wang, Yao, Ishutov, Sergey, Zambrano-Narvaez, Gonzalo, Hodder, Kevin J., Chalaturnyk, Rick J., Sun, Shuyu, Liu, Jianjun, Gamage, Ranjith P., 2020. A comprehensive experimental study on mechanical behavior, microstructure and transport properties of 3D-printed rock analogues. Rock Mech. Rock Eng. 53, 5745–5765.

Song, Rui, Wang, Yao, Sun, Shuyu, Liu, Jianjun, 2021. Characterization and microfabrication of natural porous rocks: From micro-CT imaging and digital rock modelling to micro-3D-printed rock analogues. J. Pet. Sci. Eng. 205, 108827.

Stalder, Aurélien F., Melchior, Tobias, Müller, Michael, Sage, Daniel, Blu, Thierry, Unser, Michael, 2010. Low-bond axisymmetric drop shape analysis for surface tension and contact angle measurements of sessile drops. Colloids Surf. A 364 (1–3), 72–81.

Suzuki, Anna, Watanabe, Noriaki, Li, Kewen, Horne, Roland N., 2017. Fracture network created by 3-D printer and its validation using CT images. Water Resour. Res. 53 (7), 6330–6339.

Tompson, Andrew F.B., Gelhar, Lynn W., 1990. Numerical simulation of solute transport in three-dimensional, randomly heterogeneous porous media. Water Resour. Res. 26 (10), 2541–2562. http://dx.doi.org/10.1029/WR026i010p02541, arXiv:https://agupubs.onlinelibrary.wiley.com/doi/pdf/10.1029/WR026i010p02541, URL https://agupubs.onlinelibrary.wiley.com/doi/abs/10.1029/WR026i010p02541.

Valocchi, Albert J., Bolster, Diogo, Werth, Charles J., 2019. Mixing-limited reactions in porous media. Transp. Porous Media (ISSN: 1573-1634) 130 (1), 157–182. http://dx.doi.org/10.1007/s11242-018-1204-1.

Vogel, H.-J., Roth, K., 2001. Quantitative morphology and network representation of soil pore structure. Adv. Water Resour. 24 (3–4), 233–242.

Vogelsang, David, Adriaensens, Peter, Wyns, Kenny, Michielsen, Bart, Gys, Nick, Mullens, Steven, 2022. Silanization of 3D-printed silica fibers and monoliths. ACS Appl. Mater. Interfaces 14 (25), 29345–29356.

Werth, Charles J., Cirpka, Olaf A., Grathwohl, Peter, 2006. Enhanced mixing and reaction through flow focusing in heterogeneous porous media. Water Resour. Res. 42 (12), http://dx.doi.org/10.1029/2005WR004511, 2005WR004511 (ISSN 0043-1397, 1944-7973) URL https://agupubs.onlinelibrary.wiley.com/doi/10.1029/2005WR004511.

Woche, S.K., Goebel, M.-O., Kirkham, M.B., Horton, R., Van der Ploeg, R.R., Bachmann, J., 2005. Contact angle of soils as affected by depth, texture, and land management. Eur. J. Soil Sci. 56 (2), 239–251.

Xiong, Qingrong, Baychev, Todor G., Jivkov, Andrey P., 2016. Review of pore network modelling of porous media: Experimental characterisations, network constructions and applications to reactive transport. J. Contam. Hydrol. (ISSN: 01697722) 192, 101–117. http://dx.doi.org/10.1016/j.jconhyd.2016.07.002, URL https://linkinghub.elsevier.com/retrieve/pii/S016977221630122X.

Ye, Jun, Lin, Xiaoyang, Lu, Hongjia, Shen, Hongyao, Wang, Zhen, Zhao, Yang, 2024. Layout and geometry optimization design for 3D printing of self-supporting structures. Structures (ISSN: 23520124) 59, 105699. http://dx.doi.org/10.1016/j.istruc.2023.105699, URL https://linkinghub.elsevier.com/retrieve/pii/S2352012423017873.

Zheng, Chunmiao, Bianchi, Marco, Gorelick, Steven M., 2011. Lessons learned from 25 years of research at the MADE site. Groundwater 49 (5), 649–662. http://dx.doi.org/10.1111/j.1745-6584.2010.00753.x, arXiv:https://ngwa.onlinelibrary.wiley.com/doi/pdf/10.1111/j.1745-6584.2010.00753.x, URL https://ngwa.onlinelibrary.wiley.com/doi/abs/10.1111/j.1745-6584.2010.00753.x.